JOURNAL OF CATALYSIS **178,** 338–351 (1998)
ARTICLE NO. CA982104

Evolution of the Catalytic Activity in Pt/Sulfated Zirconia Catalysts: Structure, Composition, and Catalytic Properties of the Catalyst Precursor and the Calcined Catalyst

Jean-Marie Manoli,* Claude Potvin,* Martin Muhler,†,[1] Ute Wild,† Gábor Resofszki,‡ Thomas Buchholz,§,[2] and Zoltán Paál§,[3]

*Laboratoire de Reactivité de Surface, URA 1106, casier 178, Université P. & M. Curie, F-75252 Paris Cedex 05, France; †Fritz-Haber-Institut der Max-Planck-Gesellschaft, Berlin, Faradayweg 4-6, D-14195 Germany; ‡Hungarian Oil and Gas Co., Százhalombatta, P.O. Box 1, H-2443 Hungary; and §Institute of Isotopes of the Hungarian Academy of Sciences, Budapest, P.O. Box 77, H-1525 Hungary

Received November 18, 1997; revised April 8, 1998; accepted April 8, 1998

A 3% Pt/sulfated zirconia catalyst was prepared and characterized before and after calcination at 900 K by XRD, XPS, EM, and in the catalytic hydroisomerization of *n*-hexane. The "fresh" sample exhibited small but definite catalytic properties. Calcination brought about a dramatic increase of the activity with practically constant high (90–100%) selectivity for hydroisomerization versus cracking. This increased activity was accompanied by the transformation of the predominantly amorphous support to predominantly tetragonal crystals and the wrapping up of most parts of surface Pt atoms into the bulk, as shown by the physical characterization methods. Hence metallic Pt particles exhibited mainly Pt–O rather than Pt–S interactions. S was present as sulfate. Pt-sulfated zirconia was different from traditional bifunctional metal catalysts on acidic supports. We attributed its higher catalytic activity and favorable isomerization selectivity to a few but very active centers, formed by interaction of Pt sites with sulfate groups on the high Miller-index surfaces of ZrO_2. Calcination must be essential to create these active sites. H_2 dissociating on Pt sites would provide the hydride species that are necessary for isomerization occurring on the acidic (sulfate-zirconia) part of that ensemble. We proposed the name "compressed bifunctional sites" for these centers of acid–metal cooperation. The assumption of such active sites, the maximum activity as a function of the hydrogen pressure, can also be explained in a consistent way.

INTRODUCTION

Sulfated zirconia based catalysts are very active and selective in hydroisomerization of alkanes (1). The relatively high number of papers appeared were summarized recently (2–4). Although sulfated zirconia reportedly (5) exhibits superacidic properties (10^4 times stronger that 100% H_2SO_4), the catalytic activity was no longer proportional to the acid strength above a certain level of acidity (6). Hence superacidic properties may not be directly related with isomerization activity. Sulfated zirconia catalysts deactivate rapidly (7, 8). Adding platinum group metals (8–15) or Fe–Mn (16) improved their long-term stability. The presence of hydrogen was indispensable for a sustainable isomerization (12, 13). A maximum curve was observed as a function of hydrogen pressure for butane isomerization, in a rather wide range of H_2/butane ratio (12), analogous to the H_2 pressure dependence of other Pt based catalysts (17, 18). Acidity itself cannot explain the striking changes in the catalytic properties brought about by the platinum content, for example, temperature-programmed desorption (TPD) curves of ammonia exhibited insignificant differences in the presence of Pt.

There are counterclaims in the literature concerning (i) the state of Pt (Pt metal, Pt sulfide, bulk or surface; Pt oxide, bulk or surface), (ii) its possible effect in generating stable and very active isomerization sites by, e.g., hydrogen spillover from Pt generating protonic sites (19), (iii) the nature of active sites in the presence of Pt (traditional bifunctional, superacidic), and (iv) the reason of deactivation (coking, loss of acidity, loss of surface Pt, etc.). Pt was assumed to be present mostly as Pt sulfide after reduction (20), H_2 at reduction temperature reducing supposedly some of the sulfate groups. Earlier we questioned that XPS results alone could adequately prove this statement (21). Later studies (4, 14, 21–26) pointed rather to a metallic Pt core surrounded by Pt oxide and/or sulfide as surface compounds or just adlayers.

To our best knowledge, no papers have been published monitoring the generation of the active catalyst during calcination. Following our preliminary report (27), the present paper will tackle the changes of the state of Pt in the process of activating Pt/sulfated zirconia by calcination in air

[1] Present address: Ruhr-Universität Bochum, Lehrstuhl für technische Chemie, Bochum, D 44780 Germany.

[2] On leave from Fachhochschule Ostfriesland, Constantiaplatz 4, Emden, D-26723 Germany.

[3] Corresponding author.

0021-9517/98 $25.00

at 900 K and intends to clarify its role in alkane hydroisomerization reactions. To this end, X-ray photoelectron spectroscopy (XPS), ion scattering spectroscopy (ISS), as well as X-ray diffraction (XRD) and electron microscopy (EM) have been applied, along with monitoring the catalytic properties of the dried impregnated catalyst precursor as well as that of the calcined catalysts. Further papers will tackle problems like the activity of sulfated zirconia without Pt, the initial selectivity changes, and possible reasons of temporary and final deactivation of Pt-sulfated zirconia, as well as their likely Pt–S interactions.

EXPERIMENTAL

Surface Analysis

A Leybold LHS 12 MCD instrument, equipped with X-ray source (Mg K_α or Al K_α anode) and ion gun for ISS was used for surface analysis (28–30). Dry powdered samples placed on a stainless steel sample holder or suspensions in methanol or *n*-hexane dropped to the sample holder and dried were equally suited. Samples could also be subjected to *in-situ* reduction at near-atmospheric pressure in the preparation chamber at 380°C (653 K) and the letter H is added to their code. The samples showed a BE shift of 6–7 eV due to electrostatic charging. We used the Si 2p peak of the minor SiO_2 content for BE calibration, BE = 103.3 eV (31, 32). TUBUS experiments (32) with 45-V bias were also carried out with one of the samples causing a BE shift of ca 20–25 eV. After energy calibration, the peak BE values agreed within a few tenths electron volts with those measured without TUBUS, indicating that no inhomogeneous charge occurred. For samples taken out of the catalytic reactor, with a possible glass wool contamination (in which the Si peak may have carried a different electrostatic charge) the binding energy values were normalized for Zr in ZrO_2, BE = 182.7 eV (34). The SciPlot software (© M. Wesemann, Fritz-Haber-Institut) was used for spectrum evaluation: satellite background subtraction, Shirley background subtraction, and integration (28–30), using literature values of atomic sensitivity factors for quantitative determination of surface composition (32). He^+ ions of 2 kV were used for ISS under quasi-static conditions (28).

X-Ray Diffraction

A Siemens D500 automatic diffractometer with a Cu K_α monochromatized radiation source was used for determination of the X-ray diffraction (XRD) patterns of various solid phases. The crystallite dimensions were determined using the Scherrer equation: $D_{(hkl)} = 0.9\ \lambda/B \cos\theta$, where $D_{(hkl)}$ is the crystal thickness in the hkl direction, λ is the wavelength of the X-ray diffraction, B is the peak width at half-maximum corrected for instrumental broadening, and θ is the Bragg angle of the diffraction peak. The peak intensities were fitted by a pseudo-Voight function, assuming a linear background. The standard error was ~±5%.

Electron Microscopy

The samples were ground, dispersed in ethanol in an ultrasonic bath, and deposited on a thin carbon film supported on a standard copper grid. HRTEM studies were performed on a JEOL apparatus (JEM 100 CXII) equipped with a top entry device and operating at 100 kV. The camera length was calibrated with polycrystalline gold powder.

Catalytic Runs

The activity tests were carried out in a laboratory closed-loop glass circulation reactor (28–30), at an *n*-hexane pressure of 10 Torr with the H_2 pressure varying between 60 and 480 Torr. The sampling time was between 5 and 240 min. Regeneration with circulating gases: oxygen (followed by evacuation) and hydrogen took place between runs. A fused quartz column coated with CP Sil-5 was used for GLC analysis, ensuring separation between methane and benzene (28–30). Preliminary catalytic tests were carried out after preparation in a single-pass reactor at atmospheric pressure with 10 Torr *n*-hexane in N_2.

RESULTS

Catalyst Preparation

$ZrOCl_2 \cdot 8H_2O$ was hydrolyzed by NH_4OH to get zirconium hydroxide. Gmelin's *Handbook of Inorganic Chemistry* regards this as a hydrated zirconium oxide rather than a stoichiometric compound. It was necessary to add more than 2 moles of ammonia (equivalent to the Cl content of the parent compound) to reach a basic final pH after precipitation resulting in active catalysts (Table 1). Adding ~3 moles NH_4OH per mole of $ZrOCl_2$ was necessary to

TABLE 1

Ammonia Excess, Final pH at Precipitation of Zr Hydroxide, and the Activity of Catalysts after Calcination[a]

NH_4OH excess	Final pH	Relative activity[b]
1.2	2.0	—
1.9	4.0	—
2.2	6.0	0.45
2.4	7.0	—
2.5	8.0	0.85
3	9.0	0.90
6	10.0	0.77

[a] Selected values from 60 parallel experiment. At least 3 and at most 8 parallel points have been measured for each line.

[b] Characterized by the overall conversion measured after 50 min time-on-stream in a flow reactor at 423 K, with 10 Torr *n*-hexane in N_2 carrier gas over samples subjected to calcination at 900 K.

reach a pH of 8–9, which is optimum for the subsequent catalytic activity of sulfated zirconia. A sixfold excess of ammonia was necessary to reach the value of pH = 10 reported by Yori *et al.* (7). This latter sample was less active in our case (Table 1).

The support was then treated with H_2SO_4. An optimum SO_3 content was reached when the concentration of H_2SO_4 was 0.5N. This 0.5N sulfuric acid was applied in a fivefold excess related to Zr oxide hydrate. The sample was then dried at 373 K. At this drying temperature, the H_2SO_4 uptake was 10 mol% accompanied by a loss of 3% Zr, as opposed to an H_2SO_4 uptake of 17% after a drying at 323 K, which gave much higher Zr loss (10%). Drying at 403 K, in turn, resulted in an H_2SO_4 uptake as low as 2%.

Pt was introduced by suspending the dried sulfated zirconia with a 0.15N $PtCl_4$ solution (25). It was then reduced in H_2 at 373 K (code: "fresh"). The H_2O/ZrO_2 ratio in this sample was 1.15 as opposed to the value of 1.4 after drying at 323 K and the value of 0.65 after drying at 403 K. It contained about 3% Pt to facilitate detection of Pt by XPS. To obtain an active catalyst, the dried and reduced sample was calcined in air at 900 K (code: "calc.") according to a program: the temperature was raised up to 573 K within 1 h, kept at 573 K for 1 h, the subsequent heating up to 900 K lasted for 5 h, followed by an isothermal period of 3 h. Finally, the sample was left alone to cool. The absorption and titration of SO_3 leaving the sample during calcination showed the removal of 23% of the original SO_3 content. The weight loss indicated a water removal of 12 w/w% of the original Zr oxide-hydrate; about 2/3 of the total water loss occurred below 523 K. The drying temperature influenced the activity of the subsequently calcined sample: that dried at 373 K had a higher activity by a factor of 1.2–1.5 than those dried at lower temperatures; drying at 403 K gave an inactive sample after calcination.

Electron Microscopy

Electron microscopy showed some well-characterized Pt particles in the fresh state, together with smaller Pt ones. Figure 1 shows a larger particle whose lattice fringes correspond to those of the Pt(111) plane (the magnification applied in print cannot reproduce these). Pt particles show a somewhat weaker contrast after calcination (Fig. 2) but

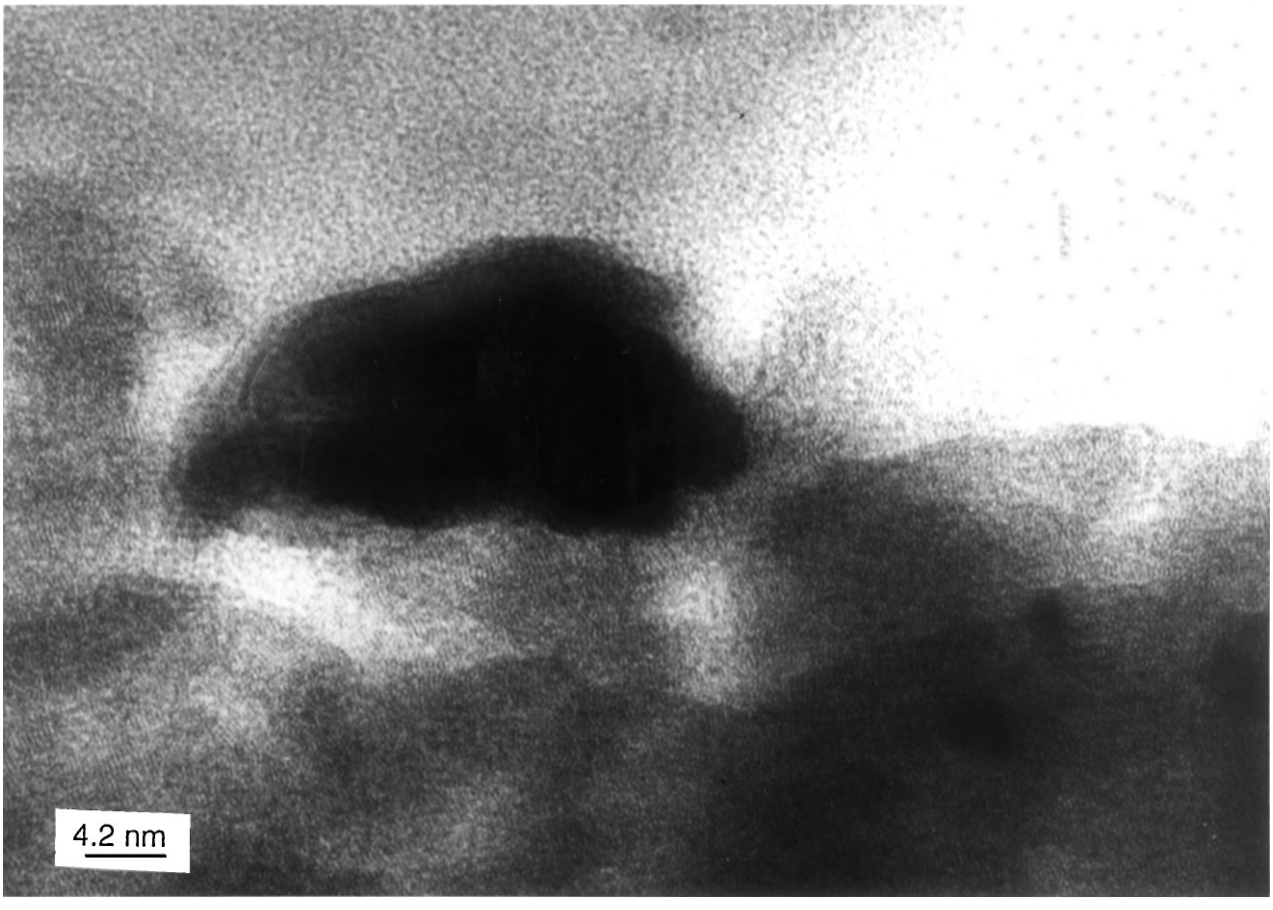

FIG. 1. Electron micrograph of a "fresh" Pt/sulfated zirconia catalyst sample. Note the occurrence of lattice fringes on the large aggregate of Pt particles. The interfringe distances correspond to that of Pt(111).

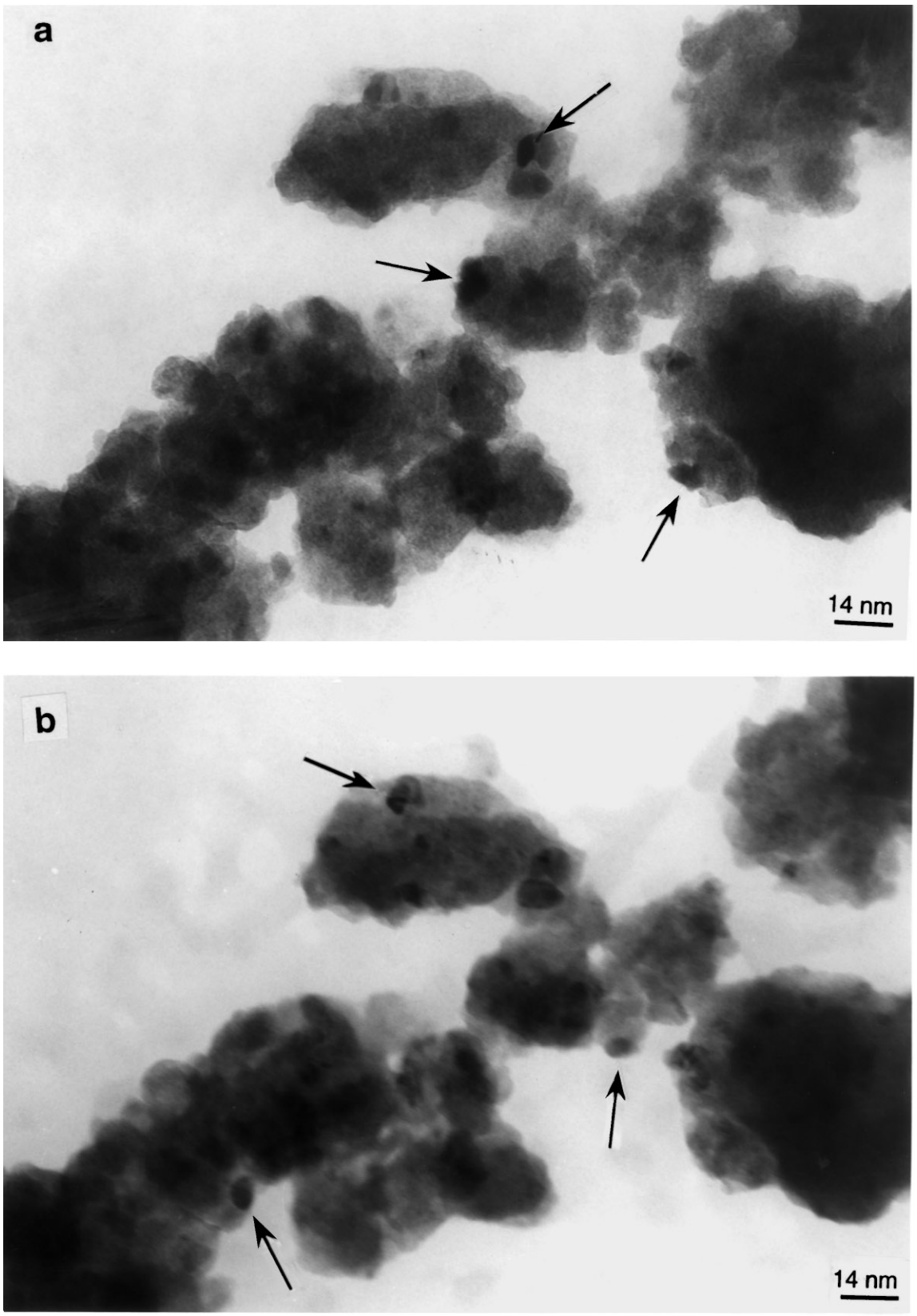

FIG. 2. Restructuring of a "calc." Pt/sulfated zirconia catalyst under the electron beam: (a) first electron micrograph after placement under the beam; (b) last electron micrograph after having kept the sample under the beam for several minutes. Arrows denote crystallites where reconstruction, disappearance (a), reappearance (b) of Pt particles were observed.

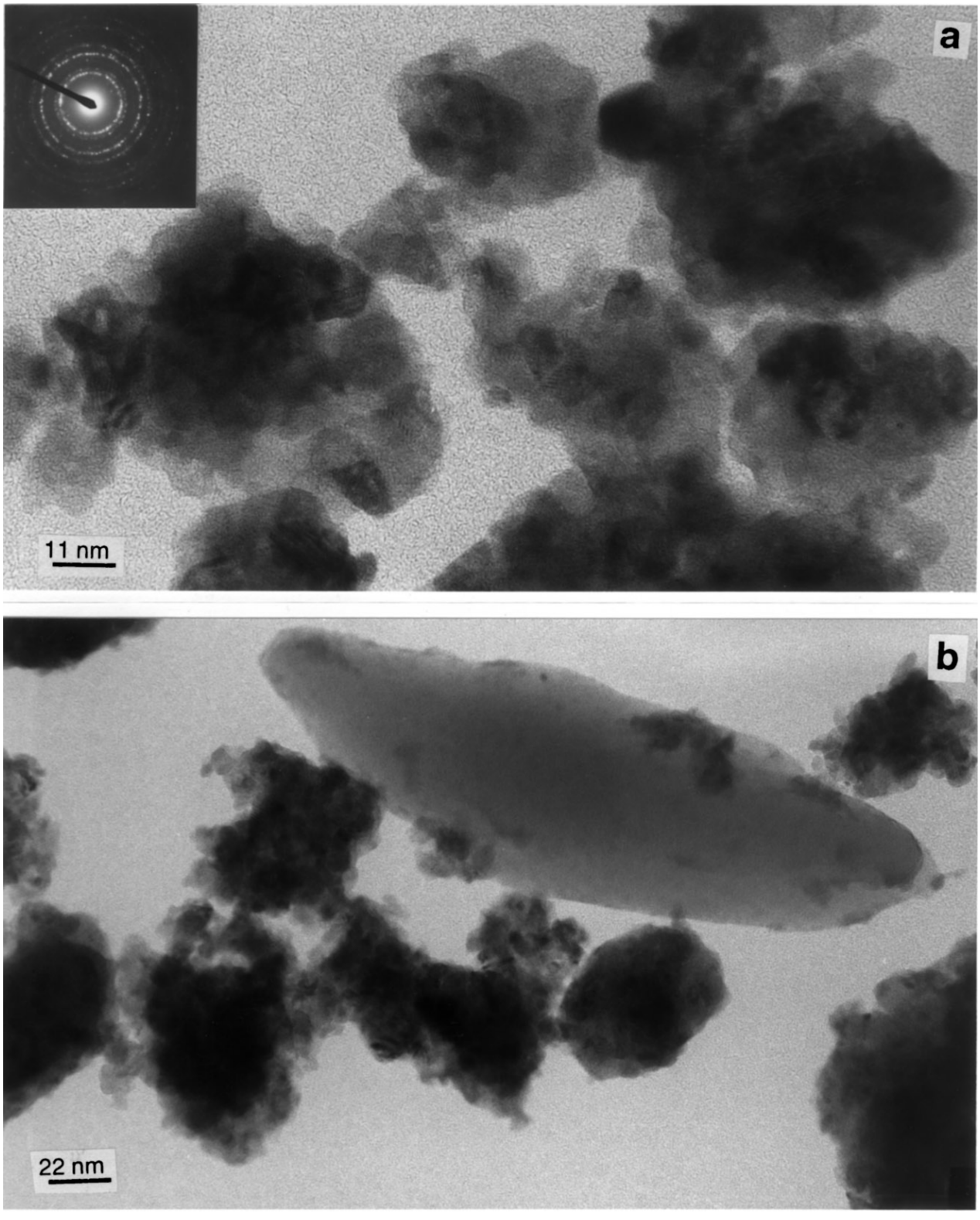

FIG. 3. Electron micrographs of areas showing mainly support. (a) support with finer crystal structure, exhibiting excellent diffraction rings (inset) corresponding to tetragonal ZrO_2, in particular, a d-spacing of 0.209 nm corresponding to the (112) plane missing in the cubic form; (b) area with a large amorphous support grain exhibiting no diffraction pattern at all.

their size—*as appeared in the electron microscope*—was not very different from those observed in the fresh sample. The particles were too small to be identified by lattice fringes. Some dark spots that may correspond to Pt particles undergo changes during exposure to the electron beam: some disappear, some gain a sharper contrast, and some appear anew, as illustrated by the comparison of the same area depicted in Figs. 2a and 2b.

Smaller ZrO_2 particles were seen, together with larger ones in the "calc." catalyst (Fig. 3). The small particles showed sharp electron diffraction rings, corresponding to well-crystallized tetragonal ZrO_2, whereas some amorphous larger particles were also seen.

X-Ray Diffraction

The X-ray diffraction pattern (Fig. 4) of the "fresh" catalyst shows well-defined narrow lines of Pt, together with broad and indistinct lines for zirconia, indicating its low crystallinity. After calcination, intense zirconia lines corresponding to tetragonal zirconia (JPCD file No. 17-0923) appear. No lines corresponding to monoclinic zirconia were seen and the presence of cubic zirconia could also be excluded. The most intense ZrO_2 line in the spectrum of the "calc" sample (line b, Fig. 4) at 2θ–30° is clearly seen to be superimposed to a broad, poorly defined amorphous background (line a) and this confirms the coexistence of amorphous and crystalline zirconia. The Pt lines after calcination were broader and less intense. The fitting of the Pt line at 2θ–40° gave a peak area about twice as high with the "fresh" sample than with the "calc." one. Thus, the redispersion of Pt was more clearly evidenced from XRD than observed by electron microscopy.

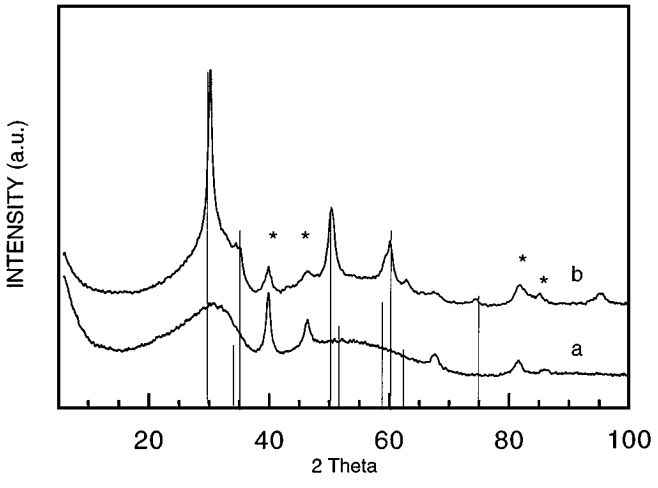

FIG. 4. X-ray diffraction pattern of Pt/sulfated zirconia catalysts in the "fresh" (a) and "calc." (b) states. The recrystallization after calcination (curve b) is clearly shown by the appearance of lines for tetragonal ZrO_2 (JPCD 17-0923) depicted as vertical lines with lengths proportional to the corresponding intensities. The diffraction lines of Pt metal (JPCD 4-0802), denoted by asterisks are also clearly distinguishable in both cases, but they are more marked with the "fresh" catalyst.

TABLE 2

Surface Composition of Pt/Sulfated ZrO_2 Catalyst Samples[a]

Sample	Composition, %					
	O	Zr	S	C	Si	Pt
Fresh[b]	57.4	18.2	3.3	12.3	5.4	2.5
Fresh/H[c]	59	21.7	2.7	7.2	6.0	3.3
Fresh/nH[d]	55.4	17	3.3	13	9.3[e]	2
Fresh/nH/H[c,d]	57	19.1	3	9.6	9[e]	2.3
"Calc."	68.4	22.1	4.5	1.4	3.1	0.42
"Calc."/H[c]	65.5	23.1	3.5	4.2	3.3	0.4

[a] As determined from the areas of the O 1s, Zr 3d, S 2p, C 1s, Si 2p, and Pt 4f lines, using sensitivity factors taken from the literature (32).
[b] 0.9% Cl impurity.
[c] H means an *in-situ* hydrogen treatment at 653 K.
[d] nH means a catalyst used for several subsequent catalytic runs in *n*-hexane–hydrogen mixtures (summarized length of runs up to 8 h).
[e] Glass wool contamination possible.

XPS of "Fresh" and "Calcined" Catalysts

Composition. The composition of both samples was similar—except for the values for Pt (Table 2). Calcination removed a large fraction of carbon impurity, which adsorbed, likely, from pollution present in surrounding air. An *in-situ* hydrogen treatment of both the "fresh" and "calc" samples removed a small fraction of carbon, increased somewhat the Pt concentration; otherwise it did not influence markedly the overall composition. After having used the "fresh" sample in catalytic reactions, its carbon content increased (Table 2), leaving the other components almost unchanged. Hydrogen treatment removed some of this carbon, too. The small Cl impurity of the "fresh" sample originating from impregnation with hydrogen chloroplatinate disappeared even after *in-situ* hydrogen treatment at 650 K.

The Pt content of "fresh" catalyst corresponded roughly to its nominal composition of ca 3% and this remained so after *n*-hexane reactions, too. One of the most dramatic changes brought about by calcination in air at 900 K was the drop of its surface concentration by nearly an order of magnitude. The structural rearrangements accompanying this composition change must have been necessary for creation of active sites.

Oxygen. The O 1s peak showed in all cases two components (Fig. 5). One at ca 530.5 eV should correspond to ZrO_2, along with a shoulder at ca 532.5 eV. This latter can be attributed to a possible zirconium hydroxide species (34) and/or to oxygen in sulfate (31, 35). Our O 1s spectra had a similar shape as reported by Milburn *et al.* (35), although their different BE scale makes quantitative comparison difficult. This higher BE component was ca equal to the ZrO_2 peak in the "fresh" catalyst. Any heat treatment (even hydrogenation at 653 K) decreased its intensity (Fig. 5, dotted spectra). The higher BE peak was restored to some extent after *n*-hexane reactions (Fig. 5, dashed spectrum).

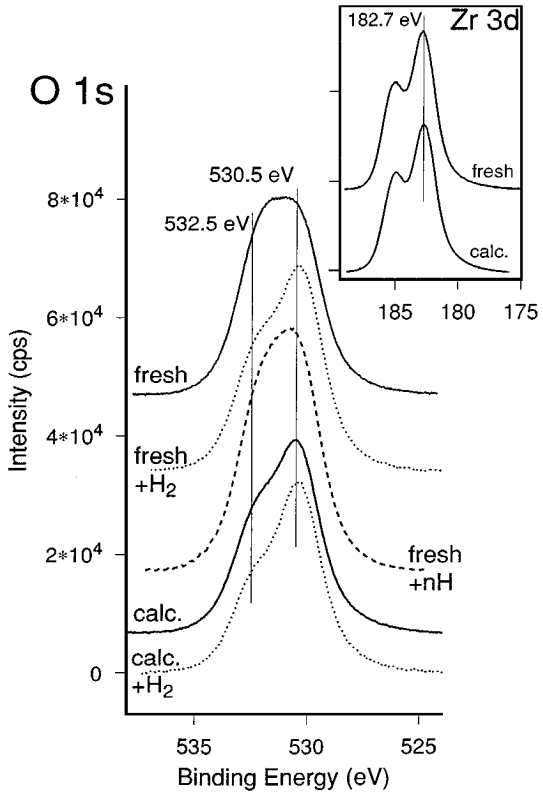

FIG. 5. O 1s region of "fresh" and "calc." catalysts in the "as received" state and after *in-situ* hydrogen treatments at 650 K (denoted by "$+H_2$"). as well as after *n*-hexane reactions on the "fresh" catalysts. Inset: Zr 3d region of "fresh" and "calc." catalysts.

Zirconium. Literature reported various BE(max) values for the Zr 3d line in ZrO_2: 182.8 eV (34); 182.9 eV (36); or 182.75 eV (37). Our values of BE = 182.7 eV measured with "fresh" and "calc." catalysts were closer to those values after energy calibration (Fig. 5, inset) than the value of BE = 182.3 eV published by other sources (20, 32). The shape of the doublet in the catalyst samples was similar after each treatment.

Sulfur. The state of sulfur (Fig. 6) corresponded in both "fresh" and "calc." catalysts to sulfate, BE = 169.5 eV (32). No changes appeared after *n*-hexane reactions. The tailing at BE ~ 165 eV may have indicated a minor reduction to S^{4+}. Thus, the redox reaction of S assumed during hydrocarbon reactions may have been stopped at this valence state. *In-situ* hydrogen reduction of the samples had given rise to some sulfide close to the detection limit, not separated reliably from spectral noise (Fig. 6, dotted spectra).

Platinum. The higher Pt content of "fresh" samples gave well-shaped Pt 4f doublet, similar to what would be expected from a supported catalyst of not too high dispersion (Fig. 7). *n*-Hexane reactions did not change the intensity or the BE position of Pt 4f. The BE of Pt 4f 7/2 in the "as received" state was around 71.8–72 eV, i.e., higher than that corresponding to metallic Pt (32). The marked drop of Pt intensity upon calcination was concomitant to a very slight BE shift. The BE was shifted to ca 71.3–71.6 eV after *in-situ* hydrogen treatment as well as after *n*-hexane reactions. This shift was somewhat more pronounced with the calcined catalyst. This indicates that Pt can be reduced by hydrogen at 650 K and its state approached that of a clean metallic Pt (BE = 71.1 eV in the same apparatus (29, 30)).

Carbon. The main carbon peak was at ca BE 284.8 eV, corresponding to hydrocarbonaceous and/or graphitic deposits (32). In the "fresh" sample, also a smaller peak appeared at ca 289 eV indicating heavily oxidized residues (COOH groups). This disappeared upon hydrogen treatment. Calcination reduced the carbon content drastically (Table 2). More carbon was present after hydrogen treatment of the "calc." catalyst, pointing to a possible reappearance of carbonaceous entities encapsulated in deeper layers during its restructuring. Carbon aggregation to three-dimensional islands could also take place under hydrogen effect (38). These contiguous carbonaceous islands were found earlier to give rise to inhomogeneous electrostatic charge (30) and could have been the reason of a BE shift of ca 0.5 eV as compared to all components but Si (corrected in the figures).

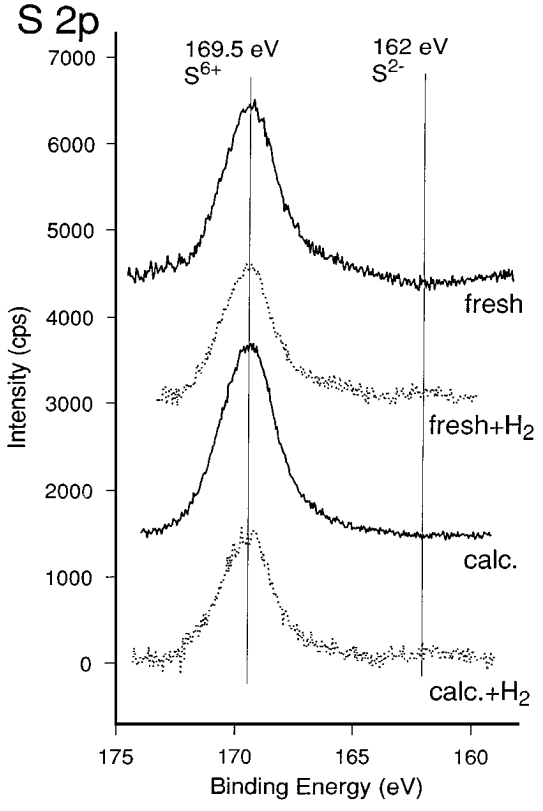

FIG. 6. S 2p region of "fresh" and "calc." samples measured in "as received" states and after *in-situ* hydrogen treatment (denoted by "$+H_2$"). Spectra taken after *n*-hexane reactions on the "fresh" catalysts were very similar to the "fresh" spectra; hence they are not shown.

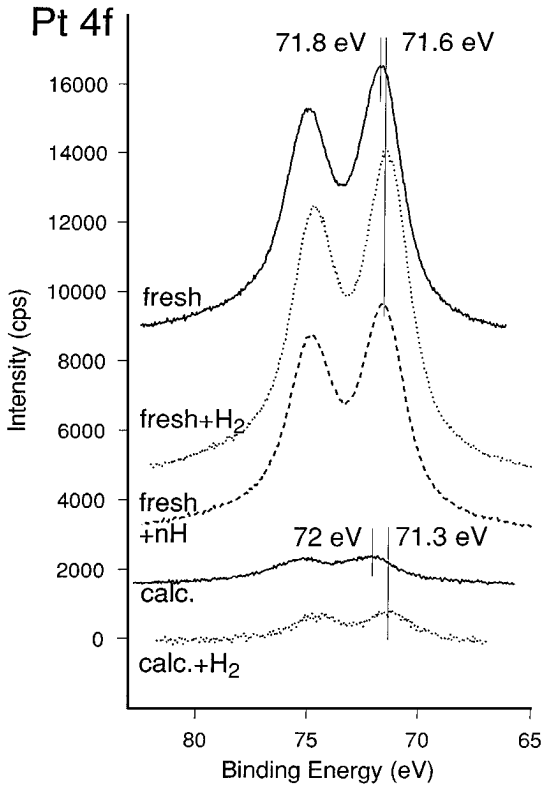

FIG. 7. Pt 4f region of "fresh," "fresh" + *n*-hexane, and "calc." catalysts, in the "as received" state and after *in-situ* hydrogen treatments at 650 K (denoted by "$+H_2$"). The intensity of the sample after *n*-hexane reactions has been measured another occasion as the other ones, and was normalized to the Pt intensity of the "fresh" catalyst by a factor of 0.67.

Silicon was regarded as an impurity and has, very likely, nothing to do with the other catalyst components.

Ion Scattering Spectroscopy (ISS)

The spectra of both "fresh" and "calc." samples gave an independent experimental evidence of their very different surface Pt concentrations (Fig. 8). The "fresh" catalyst showed a small but clearly discernible Pt signal, whereas that from the "calc." catalyst was hardly separated from the background. The spectra shown were obtained after several scans accumulated. The sputtering effect of the He^+ ions as well as the repulsion between insulating powder grains charged electrostatically under a constant impact of positive ions (which could be only partly compensated by the use of electron flood gun) thinned the sample layer so that signals from the underlying steel holder plate appeared.

Catalytic Results

Comparison of "fresh" and "calc." catalysts at various temperatures. Various supported (39–41) and unsupported (28, 29) Pt catalysts started to be active from 520–

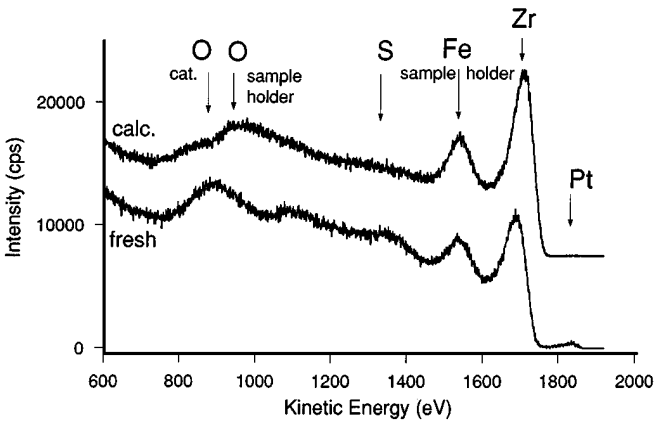

FIG. 8. Ion scattering spectra (ISS) of the fresh and calcined catalysts. He^+ ions of 2 keV were used. Cumulated results obtained in 30 subsequent scans are shown. The abrasive effect of subsequent scans wore off some of the sample and signals from the underlying sample holder became visible.

540 K upwards in "skeletal" reactions of alkanes: isomerization, C_5-cyclization, hydrogenolysis, aromatization. The "fresh" Pt/sulfated zirconia catalyst showed some activity already at ca 480 K. The "calc." sample, in turn, produced isomers already at 420 K. A much smaller mass of "calc." catalyst gave higher conversions than a higher mass of the "fresh" one (Table 3). Figure 9 shows this in terms of specific activity per ***unit mass*** of Pt. No signs of irreversible deactivation was observed even after runs up to 50 min. Sulfated zirconia without Pt showed, in turn, a short-living catalytic activity.

The selectivities as a function of the temperature (Table 3) show a similar abundance of skeletal isomers on both the "fresh" and the "calc." sample up to ca 573 K. Below 540 K, skeletal isomers (mostly methylpentanes, along with minor amounts of dimethylbutanes) were the only products. Traces of fragments and olefins also appeared at

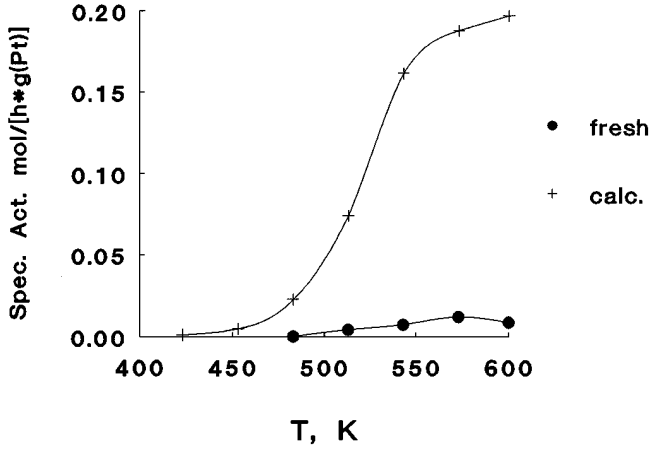

FIG. 9. Activity (mol *n*-hexane transformed per mass unit Pt per unit time) of "fresh" and "calc." Pt/sulfated zirconia catalysts as a function of the temperature: $p(nH) = 10$ Torr, $p(H_2) = 120$ Torr, sampling time, 5 min.

TABLE 3

Selectivity of *n*-Hexane Reactions on "Fresh" and "Calc." Pt/Sulfated ZrO_2 Catalysts[a] Together with Results Obtained on Other Pt Catalysts on Supports of Various Acidity

Sample	T, K	Conv., %	Selectivity, %[b]					
			$<C_6$	DMB	MP	MCP	Hex.	Bz
"Fresh"	483	0.07	0	0	100	0	0	0
	513	1.3	0	0	100	0	0	0
	543	2.2	0	9	90.2	0.8	0	0
	573	3.6	4.4	11.9	92.2	0.4	0.6	0.5
	603	2.6	19.0	10.4	67.3	0.6	2.0	0.7
"Calc."	423	0.08	0	0	100	0	0	0
	453	0.3	0	6.7	93.3	0	0	0
	483	1.5	0.4	9.4	89.8	0.4	0	0
	513	4.9	1.0	10.6	87.7	0.4	0.3	0
	543	10.6	1.8	11.7	85.6	0.5	—	0.4
	573	12.3	4.2	11.9	82.5	0.5	0.5	0.4
	603	12.9	10.1	10.9	74.8	0.6	2.6	0.9
Pt/SiO_2[c]	543	6.7	7	~1	37	49	—	6
	603	12.8	13.5		23	42.5	9	12
Pt/NaHY[d]	603	4.2	5	3	48	9	20	15
Pt/HY[d]	603	5.1	17	6	47	1	29	0

[a] 135 mg "fresh" catalyst and 29 mg "calc" catalyst.
[b] $<C_6$: fragments; DMB: dimethylbutanes; MP: methylpentanes; MCP: methylcyclopentane; Hex.: *n*-hexenes; Bz: benzene. Calculated for C_6 units transformed.
[c] 6% Pt on neutral SiO_2 support; Ref. (42).
[d] 0.8% Pt on highly acidic (Pt/HY) or slightly acidic (Pt/NaHY) support; Ref. (40).

higher temperatures. Their selectivity increased abruptly above 570 K on the "fresh" sample, whereas their amount was much lower over the "calc." catalyst. Traces of benzene and methylcyclopentane (MCP) appeared at highest temperatures. The formation of methylpentanes was favored far above thermodynamical equilibrium (Table 4). The ratio 2-methylpentane/3-methylpentane (2MP/3MP) was around 1.50, almost independently of the temperature. They were in good agreement with values obtained over Pt on slightly acidic zeolites (40, 41) but were lower than those found with Pt on neutral supports (39, 40, 42).

Fragment distribution can give information on the possible pathway of their formation. Hydrogenolysis on Pt sites gave mostly propane with less $C_5 + C_1$ fragments and even less $C_2 + C_4$ products (39, 42). Acid catalyzed cracking, in turn, gave no C_1 and C_2 fragments at all and propane prevailed (43). The fragmentation patterns obtained over Pt on zeolites of various acidity indicated that the predominance of the metal or the acid function depended strongly on the conditions, e.g., on the hydrogen excess (40, 41). Individual fragment concentrations are shown in Table 5. The "fresh" catalyst gave no methane and ethane at lower temperatures. Enhanced fragmentation at higher temperatures was due to the increase of C_3–C_5 products, including isobutane and isopentane. The "calc." sample produced small amounts of C_1–C_2 fragments. The excess of C_4 and C_5 (containing also branched fragments) with respect to the complementary C_2 and C_1 fragment was not too marked even at the highest temperature.

Catalyst stability. The XPS regions of "fresh" catalysts showed only minor structural changes after *n*-hexane reactions, due to their heating, to its interaction with *n*-hexane, or with regenerating O_2 and/or H_2 gases. This could be seen in the O 1s and Pt 4f spectra (Figs. 5 and 8), the other peaks

TABLE 4

Isomer Ratios as a Function of Temperature and Hydrogen Pressure

Catalyst	p(H_2), Torr	DMB/MP		2MP/3MP	
		543 K	603 K	543 K	603 K
"Fresh"	60	0.14	0.16	1.65	1.69
	120	0.13	0.15	1.57	1.59
	240	0.12	0.15	1.55	1.53
	360	0.09	0.15	1.49	1.50
	480	0.09	0.14	1.49	1.50
"Calc."	60	0.14	0.15	1.57	1.60
	120	0.13	0.15	1.52	1.54
	240	0.12	0.14	1.49	1.50
	360	0.11	0.14	1.46	1.49
	480	0.10	0.13	1.45	1.48
Equilibrium		0.800[a]	0.635	2.02[a]	1.95

[a] Interpolated value.

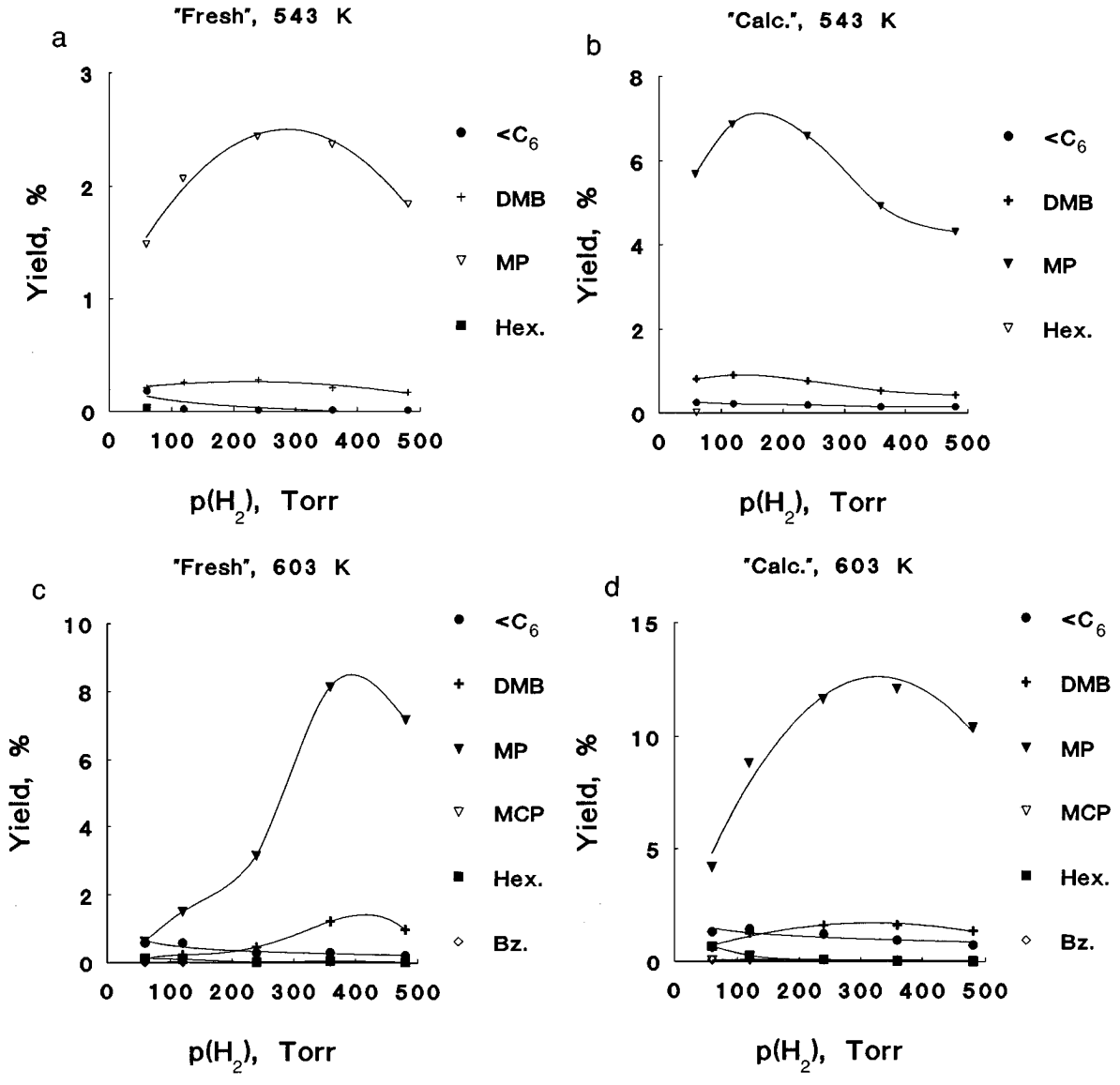

FIG. 10. Yields of individual products as a function of the hydrogen pressure: (a) "fresh" catalyst, 543 K; (b) "calc." catalyst (543 K); (c) "fresh" catalyst, 603 K; (d) "calc." catalysts, 603 K. p(*n*H) = 10 Torr, sampling time, 5 min., T = 603 K.

(Zr, S) remained almost unchanged. Some carbon accumulation occurred (Table 2). The "calc." sample showed a remarkable stability of activity and selectivity but the fresh sample exhibited a "running-in" behavior, the overall conversion increasing from Run 1 to Run 5 by a factor of 2.5 with the isomerization selectivity increasing from 83 to 92%.

Hydrogen pressure effects. The yields of skeletal hydrocarbon reactions showed, as a rule, maxima as a function of the hydrogen pressure (17, 18, 39, 40). The same was reported for butane isomerization of Pt/sulfated zirconia (12). Figure 10 illustrates characteristic differences between the yields obtained over "fresh" and "calc." samples. At 543 K (Figs. 10a and b), with mostly isomerization, both samples show shallow maxima in yields, hexene being noticeable at the lowest hydrogen pressure only. The higher activity of the "calc." sample is obvious in the whole range. Traces of MCP and (for the "calc." sample, of benzene) accompanied the main products. At 603 K (Figs. 10c and d), low hydrogen pressures favor fragmentation and dehydrogenation to olefins in both cases. The effect is much more marked with the "fresh" catalyst. Isomerization prevailed at higher hydrogen pressures. The isomer production showed maxima in all four cases as a function of $p(H_2)$. The sharp increase of yields at 603 K on the "fresh" sample above $p(H_2) = 360$ Torr is worth mentioning. The shift of the maxima towards higher hydrogen pressures with increasing temperatures appeared, here, too, as with other Pt catalysts (17, 18, 39). Increasing hydrogen pressure de-

creased the DMB/MP and the 2MP/3MP ratios on both catalysts (Table 4). The fragment distribution—normalized to 100% fragments (Table 5)—showed propane, butane(s), and pentane(s) as the main products. The "calc." catalyst produced more methane and ethane at lower temperatures. Increasing $p(H_2)$ gave rise to less butane plus pentane and more propane on both catalysts but isobutane and isopentane prevailed within the C_4–C_5 fraction.

DISCUSSION

Structure of Active Sites in the "Fresh" and Calcined Catalysts

Sulfated zirconia is regarded as a strongly acidic catalyst, exhibiting Bronsted-acid sites such as OH/H_2O attached to sulfate groups and Lewis-acid sites as coordinatively unsaturated Zr ions surrounded by sulfate groups (4, 11, 13, 44–47). There seems to be an optimum degree of hydration (around 1.1 mol H_2O/ZrO_2) and sulfation (ca 10 mol%). Calcination of our samples seem to have transformed most of the zirconia content to catalytically active (45, 46) tetragonal ZrO_2 (Fig. 4). The O 1s doublet, similar to that reported for ZrO_2 reduced in hydrogen plasma (48), may indicate the presence of a large number of ZrOH groups (BE(max.) ~533 eV (49)), together with sulfate groups (35). The atomic ratio of O/S being much higher than unity (Table 2) indicates that Zr hydroxide must have been the major component and the sulfate the minor component. The O 1s region of the "fresh" catalyst after *n*-hexane reactions (Fig. 5) may have indicated some rehydroxylation during repeated oxygen–hydrogen regenerations between catalytic runs.

No detectable reduction of sulfate to give Pt sulfide (20, 23, 24) occurred. EM showed no signs of PtS particles, as opposed to $Pt/MoO_x/Al_2O_3$ (50). Thus, S was present exclusively as sulfate in the active catalyst.

Although electron microscopy cannot monitor the presence of ultrafine Pt particles, the decrease of particle size is shown by XRD (Fig. 4). Had these smaller Pt particles been evenly distributed on the surface or had they obtained a raft-like surface structure, the XPS intensity of Pt would have *increased*. Instead, the marked loss of Pt intensity may indicate that a considerable fraction of Pt particles were "embedded" into sulfated zirconia; i.e., they were partially covered by the support, as reported for Pt/ZrO_2 (51) as well as for Pt/sulfated zirconia (52). This was confirmed also by present ISS results (Fig. 8) as well as by ISS of similar samples (27). The in-beam reconstruction has been evidenced also by EM indicating the appearance or disappearance of Pt crystallites without influencing dramatically their shape or size (see the twin in the middle of the Fig. 2 which kept its shape although its exposition changed). As far as we know, the effect of this dramatic solid-state rearrangement of Pt/sulfated zirconia on the state and distribution of platinum is being reported for the first time.

TABLE 5

Fragment Distribution over "Fresh" and "Calc." Pt/Sulfated ZrO_2 Catalysts as a Function of the Temperature and Hydrogen Pressure,[a] Together with Results Obtained on Other Pt Catalysts[b]

Sample	T, K	p(H_2), Torr	Fragment composition, %[c] C_1	C_2	C_3	C_4	C_5	Ref.
"Fresh"	543	120			51	31 (31)	18 (18)	This work
	573	120			45	33 (24)	22 (14)	
	603	60	4	4	46	32 (15)	14 (9)	
		120	—	3	48	31 (19)	18 (11)	
		480	11	6	66.5	10 (5)	6.5 (3.5)	
"Calc."	543	120	10.5	6	54	15.5 (7.5)	14 (7)	This work
	573	120	7	5	60	17 (11)	11 (8)	
	603	60	1.5	3	62	16 (12)	17.5 (13)	
		120	2.5	4	69	10.5 (10)	14 (10)	
		480	8	5.5	74.5	3 (3)	9 (7)	
Pt/SiO_2[d]	603	120	35	20	20	13 (0)	12 (0)	42
Pt/NaY[d]	603	120	46	6	15	12 (0)	21 (0)	40
Pt/NaHY[d]	603	120	21	10	16	14 (1)	39 (6)	40
		480	25	10	22	13 (0)	30 (0)	40
Pt/HY[d]	603	120	11	3	45	27 (21)	14 (8)	40

[a] Sampling time, 5 min., p(*n*H) = 10 Torr.

[b] Conversion values, X, see Table 3 for Pt/sulfated zirconia catalysts. X = 8% for Pt/SiO_2 and around 4–5% for the zeolite supported ones.

[c] Normalized to $\sum$(fragments) = 100%. In brackets: branched fragment, isobutane or isopentane (in the same units) within the total amount of C_4 and C_5 displayed.

[d] Recalculated values after original data serving as a basis for the references indicated.

The chemical state of Pt did not correspond to that of pure Pt^0 (Fig. 7). The model of metallic Pt particles surrounded by an adsorbed overlayer (14, 22–26) would agree better with our results (27). Pt–O, rather than Pt–S interactions are likely both in the "fresh" and "calc." samples (Fig. 7) in the "as received" state. The structural changes shown by EM and especially by XRD (Figs. 1 to 4) indicate that these are brought about by Pt and support oxygen ions in atomic closeness (27), similarly to recent excellent EXAFS studies of supported Pt catalysts (53, 54), where the "short" Pt–O bonds mean a direct Pt–support interaction. After calcination, several such "short" Pt–O bonds must be present. *In-situ* hydrogen reduction brought the Pt 4f 7/2 BE closer to that of the metallic state, because it could be inserted *between* the Pt and support interface, splitting some of these Pt–O bonds. This explains why the BE of Pt was closer to Pt^0 in the "calc." sample, the remaining Pt–O bonds causing still some shift (Fig. 7). Most of the Pt surface being surrounded by support species may explain the apparent hindered hydrogen chemisorption (13, 19). This structure could explain the presence of Pt–O bonds demonstrated by EXAFS in a paper which appeared after submitting the first draft of the present study (55). It attributed this structure to Pt with an O overlayer. Figure 11 offers an alternative explanation for the structure of Pt-sulfated zirconia ensembles after calcination showing Pt particles surrounded almost totally by the support. It may have been just the "fresh" sample where some Pt was interacting with support OH groups and/or H_2O which were found to be stable on Pt surface, too (29, 38). Our model explains the drastic drop of Pt intensity upon calcination (Figs. 7, 8) and does not contradict to the facts of Ref. (55).

Redispersion at the same time gives rise to few but very active sites, as shown by the increase of activity per unit mass of Pt (Fig. 9). These sites may be analogous to the small Pt ensembles anchored by a proton to a zeolite framework (41, 56). These entities may have catalyzed bifunctional reactions without shuttling the intermediates in the gas phase (40, 41). Some of the catalytic properties of the zeolitic samples (40–42) have also been included in Tables 3 and 5.

With a stronger acid like sulfated zirconia, a concerted metal–acid catalysis may prevail. Sachtler *et al.* (57) called those combined active ensembles "collapsed bifunctional sites." We prefer the word "compressed bifunctional sites" to avoid the meaning of "ruin" or "decay" for "collapse"—these sites are not ruined; on the contrary they get new force by being compressed. These sites ***do need*** neighboring Pt and sulfate (and/or sulfate-activated Zr) sites. Not *all* sulfate species may fulfill this requirement, all the more that the surface abundance of sulfate groups is higher than that of Pt (Table 2). SO_4^{2-} was shown to stabilize small tetragonal ZrO_2 crystallites on well-faceted particles and even inducing their faceting in the (110) direction (58). Thus, most of SO_4^{2-} groups would only be spectator species and a small

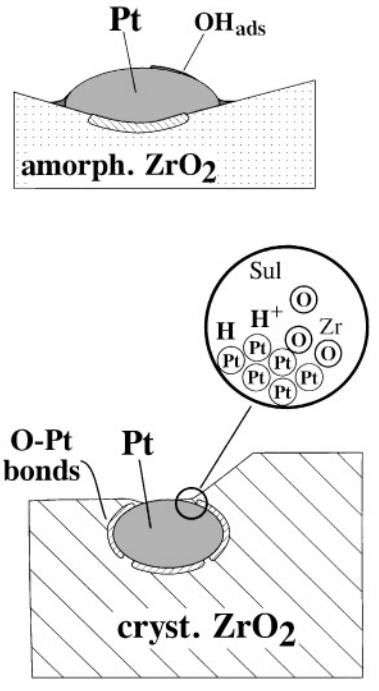

FIG. 11. Proposed structure of the Pt-sulfated zirconia catalysts before calcination (upper panel); and after calcination (lower panel). The drawing is largely symbolic, and not to scale, apart from indicating the decrease of the size of Pt particles in the "calc." sample. Patches of adsorbed OH (partly migrating from the strongly hydrated zirconia) are assumed on the larger Pt particles of the "fresh" sample. The lower panel illustrates the wrapping most Pt under the zirconia. The sulfated character of the support is not indicated in the figure, since Fig. 4 gives only evidence on ZrO_2 recrystallization. The shift of BE(max) values of Pt 4f spectra (Fig. 7) can be attributed to atomic interaction of most of the interfacial Pt atoms with support O atoms in those particles (shown by shading, not to scale) rather than to covering Pt by an O adlayer (55). The inset of the lower panel gives a very rough illustration on the atomic scale for the "compressed bifunctional sites" emerging at the metal–support borderline. They should involve a neighboring sulfate entity as shown by "Sul," without attempting to reproduce the disputed (2, 3, 46, 58) molecular structure of the latter.

number of ZrO_2 crystallites with high Miller-index surfaces would give rise to a few highly active ***acidic*** sites. If they meet Pt sites in their close vicinity, combined active ensembles arise, as illustrated schematically in Fig. 11. Pt may also stabilize these highly active sulfate species. They need specific ZrO_2 crystal planes which are not present on the mainly amorphous zirconia in the "fresh" state exhibiting poor activity although the amount of sulfate was not very different from that found after calcination (Table 1, Fig. 6). The validity of the model is corroborated by failing to prepare an active isomerization catalyst via introducing platinum into sulfated zirconia *after* its calcination. Pt and sulfated zirconia come to the necessary vicinity by recrystallization and the necessary price to pay for creating such entities is the loss of a considerable fraction of Pt. This may be one of the reasons why the accessibility (59) and reducibility (60) of Pt becomes lower upon calcination. Our idea on wrapping

up of most Pt would give an adequate explanation for these results, too, and would agree with the proposed chemical interaction (60) between Pt and support.

Effect of Hydrogen Pressure on the Catalytic Properties

Literature reported positive (11, 13, 61) as well as negative (47, 62) effect of increasing hydrogen pressure on the catalytic activity. Garin *et al.* (12) were the only ones who studied the H_2 effect in a wide pressure range and found maximum activity as a function of $p(H_2)$. Hydride transfer agents are necessary to start the isomerization reaction (13); in our case this is H_2 dissociated on metal sites. To act so, they should preserve their metallic character. Our ideas on the structure of Pt-acidic combined active ensembles agree with this assumption. The reason why the yields should have maxima as a function of hydrogen pressure are the same as was earlier proposed for metals (17, 18, 63) even if the actual steps that are promoted and hindered, respectively, by surface hydrogen may not be the same. At low H_2 pressure, the availability of hydrogen is scarce. Near maximum, there is an optimum lifetime of surface species which, in turn, is governed by the accessibility of hydrogen, as well as by the acid strength (6, 13, 57). The shift of maxima toward higher $p(H_2)$ values as temperature increases is due to the fact that higher H_2 pressures are necessary to maintain the same optimum coverage (17, 18). Too much hydrogen, in turn, competes with the intermediates on the active sites and may cause their too rapid desorption (13).

Apart from the maximum in the methylpentane (and a much shallower maximum for dimethylbutane) yields, the behavior of the catalysts changes profoundly at 603 K with changing hydrogen pressures. At low $p(H_2)$, the catalysts behave like a traditional metal supported on acidic support; dehydrogenation to olefins and cracking on acidic sites appeared, in addition to isomerization (Fig. 10). The peculiar character of metal–acid cooperation started above ~120 Torr H_2 .These active sites produced mostly methylpentanes from *n*-hexane. The surface residence time of carbenium ions must have been insufficient (13) to form isomers with quaternary C atoms as shown by the DMB/MP ratios (Table 4) being far below equilibrium. The hydrogen pressure dependence of this ratio is in agreement with the importance of optimum surface residence time; with more hydrogen present, the residence time becomes shorter and less time is available for a second isomerization step.

Although cracking was a minor reaction, yet, fragment composition may serve as still another indicator of the possible reaction routes. It revealed (Table 5) a predominant acid-catalyzed cracking. The dimeric intermediates (12, 13, 61, 62) to give C_4 and C_5 products (of these, branched ones) may be more important on the "fresh" catalysts containing less "compressed bifunctional sites." The bimolecular pathway should not be important for C_6 alkane isomerization (57). The appearance of C_1 and C_2 fragments on the "calc." sample even at lower temperature (Table 5) indicates *some* metal catalyzed hydrogenolysis along with the predominant cracking. However, considering its low activity, we do not believe that the alleged function of Pt to hydrogenolyze coke precursors (47, 61) can be important. Even higher hydrogen pressure (603 K, 480 Torr) could not bring about any metal catalyzed hydrogenolysis, as opposed to Pt/NaY (40)—see Table 5. Instead, the complementary fragments become almost equal, indicating that abundant hydrogen may have shifted the decomposition of *n*-hexane fully towards the intramolecular mechanism.

ACKNOWLEDGMENTS

Z.P. is pleased to thank Deutsche Akademische Austauschdienst (DAAD) for a fellowship to support his stay in Berlin during which the final experiments were carried out and the manuscript could be completed. The kind help of Ms. A. Hornung during this period is gratefully acknowledged. The assistance of M. Lavergne in TEM measurements as well as that of Dr. C. Németh and Ms. A. Kökény for preparing Fig. 11 is greatly appreciated.

REFERENCES

1. Olah, G. A., and Molnár, A., "Hydrocarbon Chemistry," Wiley, New York, 1995.
2. Davis, B. H., Keogh, R. A., and Srinivasan, R., *Catal. Today* **20**, 219 (1994).
3. Song, X., and Sayari, A., *Catal. Rev.-Sci. Eng.* **38**, 329 (1996).
4. Tanabe, K., and Hattori, H., *in* "Handbook of Heterogeneous Catalysis" (G. Ertl, H. Knözinger, and J. Weitkamp, Eds.), Vol. 1, p. 404. Verlag Chemie, Weinheim, 1997.
5. Hino, M., Kobayashi, S., and Arata, K., *J. Am. Chem. Soc.* **101**, 5439 (1979).
6. Adeeva, V., de Haan, J. W., Jänchen, J., Lei, G. D., Schünemann, G., van de Ven, L. J. M., Sachtler, W. M. H., and van Santen, R. A., *J. Catal.* **151**, 364 (1995).
7. Yori, J. C., Luy, J. C., and Parera, J. M., *Appl. Catal.* **46**, 103 (1989).
8. Hosi, T., Shimadzu, T., Ito, S., Baba, S., Takaoka, H., Imai, T., and Yokoyama, N., *in* "Prepr. Sym. Div. Petr. Chem. Am. Chem. Soc., 1988," p. 562.
9. Ebitani, K., Konishi, J., Horie, A., Hattori, H., and Tanabe, K., *in* "Acid-Base Catalysis" (K. Tanabe *et al.*, Eds.), p. 491, Kodansha, Tokyo, 1989.
10. Wen, M. Y., Wender, I., and Tierney, J. W., *Energy Fuels* **4**, 372 (1990).
11. Ebitani, K., Konishi, J., and Hattori, H., *J. Catal.* **130**, 257 (1991).
12. Garin, F., Andriamasinoro, D., Abdulsamad, A., and Sommer, J., *J. Catal.* **131**, 199 (1991).
13. Iglesia, E., Soled, S. L., and Kramer, G. M., *J. Catal.* **144**, 238 (1993).
14. Sayari, A., and Dicko, A., *J. Catal.* **145**, 561 (1994).
15. Vaudagna, S. R., Comelli, R. A., and Figoli, N. S., *React. Kinet. Catal. Lett.* **58**, 1 (1995).
16. Hsu, C.-Y., Heimbuch, C. R., Armes, C. T., and Gates, B. C., *J. Chem. Soc. Chem. Commun.* 1645 (1992).
17. Paál, Z., and Menon, P. G., *Catal. Rev.-Sci. Eng.* **25**, 223 (1983).
18. Paál, Z., *Catal. Today* **12**, 297 (1992).
19. Ebitani, K., Tsuji, J., Hattori, H., and Kita, H., *J. Catal.* **135**, 609 (1992).
20. Ebitani, K., Konishi, J., Tanaka, T., and Hattori, H., *J. Catal.* **135**, 60 (1992).
21. Paál, Z., Muhler, M., and Schlögl, R., *J. Catal.* **143**, 318 (1993).
22. Tanaka, T., Shishido, T., Hattori, H., Ebitani, K., and Yoshida, S., *Physica B* **208/209**, 649 (1995).
23. Ebitani, K., Tanaka, T., and Hattori, H., *Appl. Catal. A* **102**, 79 (1993).

24. Dicko, A., Song, X., Adnot, A., and Sayari, A., *J. Catal.* **150**, 254 (1994).
25. Zhao, J., Huffman, G. P., and Davis, B. H., *Catal. Lett.* **24**, 385 (1994).
26. Comelli, R. A., *Catal. Lett.* **40**, 67 (1996).
27. Paál, Z., Buchholz, T., Resofszki, G., Muhler, M., Wild, U., Manoli, J.-M., and Potvin, C., "11 Internat. Congr. Catalysis, *Baltimore, 1996*," Poster 029.
28. Paál, Z., Muhler, M., and Matusek, K., *Appl. Catal. A* **149**, 113 (1997).
29. Paál, Z., and Zhan, Z., *Langmuir* **13**, 3752 (1997).
30. Paál, Z., Xu, X. L., Paál-Lukács, J., Vogel, W., Schlögl, R., and Muhler, M., *J. Catal.* **152**, 252 (1995).
31. Moulder, J. F., Stickle, W. F., Sobol, P. E., and Bomben, K. D., "Handbook of X-Ray Photoelectron Spectroscopy," Perkin–Elmer, Eden Prairie, MN, 1992.
32. Briggs, D., and Seah, M. P. (Eds.), "Practical Surface Analysis," Appendix 6, Vol. 1, p. 635. Wiley, Chichester, 1990.
33. Muhler, M., Paál, Z., and Schlögl, R., *Appl. Surface Sci.* **47**, 281 (1991).
34. Morant, C., Sanz, J. M., Galán, L., Soriano, L., and Rueda, F., *Surf. Sci.* **218**, 331 (1989).
35. Milburn, D. R., Keogh, R. A., Srinivasan, R., and Davis, B. H., *Appl. Catal. A* **147**, 109 (1996).
36. Wang, Y. M., Li, Y. S., Wong, P. C., and Mitchell, K. A. R., *Appl. Surf. Sci.* **72**, 237 (1993).
37. Maurice, V., Salmeron, M., and Somorjai, G. A., *Surf. Sci.* **237**, 116 (1990).
38. Paál, Z., Schlögl, R., and Ertl, G., *J. Chem. Soc. Faraday Trans.* **88**, 1179 (1992).
39. Bond, G. C., and Paál, Z., *Appl. Catal. A* **86**, 1 (1992).
40. Zhan, Z., Manninger, I., Paál, Z., and Barthomeuf, D., *J. Catal.* **147**, 333 (1994).
41. Paál, Z., Zhan, Z., Manninger, I., and Sachtler, W. M. H., *J. Catal.* **155**, 43 (1995).
42. Paál, Z., Groeneweg, H., and Paál-Lukács, J., *J. Chem. Soc. Faraday Trans.* **86**, 3159 (1990).
43. Haag, W. O., and Dessau, R. M., *in* "Proceedings, 8th International Congress on Catalysis, Berlin, 1984," Vol. 2, p. 305. Verlag Chemie, Weinheim, 1984.
44. Nascimento, P., Akratopoulou, C., Oszagyan, M., Coudurier, G., Travers, C., Joly, J.-F., and Vedrine, J. C., *Stud. Surf. Sci. Catal.* **75**, 1185 (1993).
45. Morterra, C., Cerrato, G., Pinna, F., and Signoretto, M., *J. Catal.* **157**, 109 (1995).
46. Spielbauer, D., Mekhemer, G. A. H., Zaki, M. I., and Knözinger, H., *Catal. Lett.* **40**, 71 (1996).
47. Signoretto, M., Pinna, F., Strukul, G., Chies, P., Cerrato, G., Di Ciero, S., and Morterra, C., *J. Catal.* **167**, 522 (1997).
48. Wong, P. C., Li, Y. S., Zhou, M. Y., and Mitchell, K. A. R., *Appl. Surf. Sci.* **89**, 255 (1995).
49. Li, Y. S., Wong, P. C., and Mitchell, K. A. R., *Appl. Surf. Sci.* **89**, 263 (1995).
50. Paál, Z., Tétényi, P., Muhler, M., Manoli, J.-M., and Potvin, C., *J. Chem. Soc. Faraday Trans.* **94**, 459 (1998).
51a. Hoang, D.-L., and Lieske, H., *Catal. Lett.* **27**, 33 (1994).
51b. Hoang, D.-L., Berndt, H., and Lieske, H., *Catal. Lett.* **31**, 165 (1995).
52. Xue, E., Seshan, K., Mercera, P. D. L., van Ommen, J. G., and Ross, J. R. H., *ACS Symp. Series* **552**, 250 (1994).
53. Miller, J. T., Meyers, B. C., Modica, F. S., Lane, G. S., Vaarkamp, M., and Koningsberger, D. C., *J. Catal.* **143**, 395 (1993).
54. Munoz-Páez, A., and Koningsberger, D. C., *J. Phys. Chem.* **99**, 4193 (1995).
55. Shishido, T., Tanaka, T., and Hattori, H., *J. Catal.* **172**, 24 (1997).
56. Bai, X., and Sachtler, W. M. H., *J. Catal.* **129**, 121 (1991).
57. Liu, H., Lei, H., and Sachtler, W. M. H., *Appl. Catal. A* **137**, 167 (1996).
58. Benaissa, M., Santiesteban, J. G., Diaz, G., Chang, C. D., and José-Yacaman, M., *J. Catal.* **161**, 694 (1996).
59. Coq, B., Walter, C., Brown, R., McDougall, G., and Figueras, F., *Catal. Lett.* **39**, 197 (1996).
60. Ivanov, A. V., Kustov, L. M., Vasina, T. V., Kazanskii, V. B., and Zeuthen, P., *Kinet. Catal. (Eng. ed.)* **38**, 403 (1997).
61. Comelli, R. A., Finelli, R., Vaudagna, S. R., and Figoli, N. S., *Catal. Lett.* **45**, 227 (1997).
62. Sayari, A., Yang, Y., and Song, X., *J. Catal.* **167**, 346 (1997).
63. Bond, G. C., and Slaa, J. C., *J. Mol. Catal.* **98**, 81 (1995).